frontiers | Frontiers in Materials

ORIGINAL RESEARCH
published: 05 May 2022
doi: 10.3389/fmats.2022.883027

Mechanical and Antibacterial Properties of h-BN-TiO_2 Nanocomposite-Modified Glass Ionomer Cement

Yu Ma[1,2,3†], Yan-Zhu Guo[1†], Yan Liu[1], Yu-Rui Wang[1], Jiang-Chuan Yang[1], Xin-Zi Kong[1], Hong-Lin Jia[1], Rui-Zhi Li[1], Qi-Ze Han[1], Cheng-Dong Zheng[4], Xin-Jun Hu[5*] and Bin Liu[1,2*]*

[1]School and Hospital of Stomatology, Lanzhou University, Lanzhou, China, [2]Key Laboratory of Dental Maxillofacial Reconstruction and Biological Intelligence Manufacturing, Lanzhou University, Lanzhou, China, [3]Biointerfaces Institute, University of Michigan, Ann Arbor, MI, United States, [4]Clinical Research Center of Shanxi Province for Dental and Maxillofacial Diseases, College of Stomatology, Xi'an Jiaotong University, Xi'an, China, [5]School of Mechanical Engineering, Sichuan University of Science and Engineering, Zigong, China

This study investigated the mechanical properties and antibacterial properties of hexagonal boron nitride and titanium dioxide (h-BN-TiO_2) nanocomposite modified traditional glass ionomer cement. The mechanism of formation of the h-BN-TiO_2 nanocomposite was elucidated by conducting molecular dynamics (MD) simulations using the Material Studio (MS) software. Furthermore, synthesis of h-BN-TiO_2 nanocomposite by the original growth method using hexagonal boron nitride nanosheets (h-BNNs) and titanium dioxide nanoparticles (TiO_2 Nps) and characterization using TEM and AFM to determine their particle sizes, morphologies, and structures. The mechanical properties and antibacterial efficacies of the glass ionomer cement composites were analyzed based on the different mass fractions (0, 0.3, 0.7, 1.1, and 1.5 wt%) of the h-BN-TiO_2 nanocomposite. The results showed when the concentration of the h-BN-TiO_2 nanocomposite was 1.1 wt%, the Compressive strength (CS) and Vicker hardness (VHN) were 80.2% and 149.65% higher, respectively, compared to the glass ionomer cement without any h-BN-TiO_2 nanocomposite. Also, the increase in the concentration of the h-BN-TiO_2 nanocomposite led to a decrease in both the coefficient of friction (COF) and solubility, but a 93.4% increase in the antibacterial properties of the glass ionomer cement composites. The cell survival rate of each group was more than 70% after 48 h, but the difference was not statistically significant ($p > 0.05$). Therefore, the h-BN-TiO_2 nanocomposite served as a reinforcing material for glass ionomer cement, which can be useful in clinical dentistry and provide a new strategy for improving the clinical utility of glass ionomer cement.

Keywords: glass ionomer cement, h-BN-TiO2 nanocomposite, mechanical properties, antibacterial properties, molecular dynamics analysis

OPEN ACCESS

Edited by:
Marziyeh Ranjbar-Mohammadi, University of Bonab, Iran

Reviewed by:
Kawaljit Randhawa, Charotar University of Science and Technology, India
Sara Banijamali, Materials and Energy Research Center, Iran

***Correspondence:**
Yu Ma
mayu@lzu.edu.cn
Xin-Jun Hu
xjhu@suse.edu.cn
Bin Liu
liubkq@lzu.edu.cn

†These authors have contributed equally to this work and share first authorship

Specialty section:
This article was submitted to Biomaterials, a section of the journal Frontiers in Materials

Received: *24 February 2022*
Accepted: *07 April 2022*
Published: *05 May 2022*

Citation:
Ma Y, Guo Y-Z, Liu Y, Wang Y-R, Yang J-C, Kong X-Z, Jia H-L, Li R-Z, Han Q-Z, Zheng C-D, Hu X-J and Liu B (2022) Mechanical and Antibacterial Properties of h-BN-TiO_2 Nanocomposite-Modified Glass Ionomer Cement. Front. Mater. 9:883027. doi: 10.3389/fmats.2022.883027

1 INTRODUCTION

Since the 1970s, glass ionomer cement (GIC) has received significant attention as a dental restorative material in clinical practice due to its anti-caries effect, biocompatibility (Nicholson et al., 1991), excellent bonding with dentin (Nicholson, 2016; Yamakami et al., 2018), and simplicity of handling (Nicholson et al., 2020). However, GIC undergoes initial dehydration and has a high swelling rate, both of which are disadvantages that have significantly limit the mechanical and antibacterial properties of GIC (Moshaverinia et al., 2009a; Brito et al., 2010; Sun et al., 2018). To overcome these shortcomings, researchers have experimented with various methods to improve the mechanical properties of GIC. One effective method entailed incorporating organic additives, such as methacryloyl, N-vinylcaprolactam, N-vinylpyrrolidone-modified acrylic acid copolymer, and fluorapatite, into GIC to increase the mechanical strength of GIC through chemical bonding (Simmons, 1990; Moshaverinia et al., 2008a; Moshaverinia et al., 2008b; Moshaverinia et al., 2008c; Moshaverinia et al., 2009b; Moshaverinia et al., 2019; Randhawa and Patel, 2020b; Randhawa and Patel, 2020c). However, these methods are finite, and there is still significant room for improving the mechanical properties of the GIC.

In recent years, nanoflake or nanoparticle rigid materials, such as fluorapatite (FAp) nanoparticles (NPs) (Ching et al., 2018), calcium fluoride (CaF_2) (Xu et al., 2010), titanium dioxide (Zhang and Gao, 2001), and hydroxyapatite (Moheet et al., 2018), have demonstrated to be ideal candidates as nanoscale fillers, as their incorporation into dental materials has led to the effective reinforcement of dental substrates. While one study reported that adding CaF_2 nanoparticles to resin-modified GIC (RMGIC) improved the mechanical properties of the RMGIC (Moreau and Xu, 2010), the insolubility of CaF_2 reduces the ability of GIC to release fluoride. Hexagonal boron nitride (h-BN) is a 2D material like graphite, has excellent thermal, mechanical, and tribological properties (Randhawa and Patel, 2020c). Kawaljit Singh Randhawa et al. report that with the increase of content of h-BN, the COF and wear rate of composites decreased up to 4 wt% due to transfer film formation and lubricious effects of h-BN fillers (Randhawa and Patel, 2020a). Surprisingly, h-BN in nanoscale usually exhibit some unique properties in physical and chemical aspects compared with bulk h-BN materials. Some studies reported that hexagonal boron nitrides nanaosheets (h-BNNs) have received significant attention as a two-dimensional nanomaterial because of their excellent mechanical properties and biological safety (Czarniewska et al., 2019; Yue et al., 2019). In addition, h-BNNs are white powders, which enable them to be an ideal filler for medical materials, especially dental materials, with aesthetic requirements. Lee B et al. prepared boron nitride nanoplatelets/alumina (BNNP/ATZP) ceramic composites by spark plasma sintering (SPS) technology after mixing alumina powder with BNNs prepared by ball milling (Lee et al., 2020), after which a 27% increase in the bending strength of the composites, as well as a 37.5% increase in the fracture toughness, were achieved. Farooq et al. prepared a composite by functionalized hexagonal boron nitride nanosheets (h-BNNSs-OH) with polymethyl methacrylate (PMMA), which led to a 70% increase in the ultimate tensile strength (UTS) of the functionalized BN/PMMA (Farooq et al., 2020). Despite these advancements, only a few studies have investigated the addition of rigid nanomaterials to improve the mechanical properties of GIC.

Since traditional GIC are capable of releasing fluoride into the surrounding tissue, they have inherent antibacterial and anti-caries properties (Wiegand et al., 2007; Hasan et al., 2019). However, the release of fluoride would also be accompanied by the depletion of fluoride on the surface of the filling to form insoluble particles in the interior of the filling, making it inadequate to achieve long-term antibacterial effects. Recently, GIC composites have been prepared by the addition of antimicrobial agents or materials, such as dimethylamine lauryl methacrylate (DMADDM) (Zhang et al., 2015; Wang et al., 2016), chlorhexidine, and antibiotics (Abdallah et al., 2020), to increase the antibacterial and anticaries properties of the GIC (Yesilyurt et al., 2009). However, achieving a controlled rate release and the terminal depletion of drug represent the bottlenecks that limit the utility of GIC composites in clinical application. In addition, the clinical application of these materials is further restricted by the risk of drug resistance and the potential to produce superbugs (Varela et al., 2021). Thus, the development of emerging antibacterial nanomaterials would be highly advantageous to improve the antibacterial properties of GIC. Elsaka et al. reported that the addition of 2, 3, 5, and 7 wt% TiO_2 NPs to GIC was effective for inhibiting bacterial growth, and the compressive strength and microhardness of the GIC composites increased by 17% and 4%, respectively, over the unmodified GIC (Elsaka et al., 2011). Nida Hamid et al. reported that GIC containing 3 wt% TiO_2 NPs caused an increase in the inhibition rate of *Streptococcus mutans* (S.mutans) by 30% (Hamid et al., 2019). Chen B. et al. prepared ZnO/Ag hybrid microspheres that demonstrated excellent antibacterial activities, with a minimum inhibition concentration (MIC) and a minimum biotic concentration (MBC) of *Staphylococcus aureus* of 40 and 80 μg/ml, respectively (Chen et al., 2020). Since the antibacterial properties of these nanomaterials were dependent on their surface characteristics, such as the mechanical damage to bacteria caused by electrostatic forces (Hajipour et al., 2012), they exhibit long-term and non-fading antibacterial properties while eliminating the risk of bacterial resistance. While the aforementioned methods were effective for improving the antibacterial performance of GIC, there remains a lack of effective methods for synergistically improving both the antibacterial and the mechanical properties of GIC.

Given the outstanding mechanical effect of h-BNNs and the inherent antibacterial properties of TiO_2 NPs, this study investigated the combination of h-BN and TiO_2 by first-principles calculations of density functional theory. The ball-milling and the thermal hydrolysis of Titanium oxysulfate were used to prepare h-BN-TiO_2 nanocomposite to construct a two-dimensional and zero-dimensional nanocomposite system. Subsequently, the synthesized h-BN-TiO_2 nanocomposite was added to GIC in a certain proportion, aiming not only to enhance GIC effectively achieved a substantial improvement in the

mechanical and antibacterial properties of traditional GIC (**Figure 1**), but also to provide a novel insight into the development of more GIC enhancement methods.

2 MATERIALS AND METHODS

2.1 Molecular Dynamics Analysis of Hexagonal Boron Nitride and Titanium Dioxide

We utilized molecular dynamic (MD) simulations to analyze the changes in the molecular structure and reaction system energy during the recombination of h-BN and TiO_2 to better understand the reaction mechanism. Based on the first principles of density functional theory (DFT), we calculated the adsorption energy of TiO_2 (anatase type, 101 face) onto the h-BN using the Forcite$^+$ module in MS package. Three systems were constructed: 1) the anatase-TiO_2 model, 2) the monolayer h-BN model, and 3) the h-BN-TiO_2 composite model. The structural and size parameters of TiO_2 and h-BN inputted into the software program were derived from the literature and were used to optimize the geometric structures of TiO_2 (**Supplementary Figure S1, S2**) and h-BN (**Supplementary Figure S3, S4**). The initial h-BN-TiO_2 composite structure was the (101) TiO_2 surface adsorbed onto the h-BN. Simulations were carried out under the NVT ensemble, and each system was simulated for 100 ns. The adsorption energy of anatase-TiO_2 on h-BN was calculated after the reaction reached equilibrium using the following equation:

$$E = E_{h-BN-TiO_2} - \left(E_{h-BN} + E_{TiO_2}\right)$$

The adsorption energy of the TiO_2 onto the h-BN was calculated by selecting the final XML schema definition (XSD) structure of the TiO_2 and the h-BN from the MD simulations and subtracting the TiO_2 energy from the total energy of the h-BN-TiO_2 system and then subtracting the h-BN energy.

2.2 Preparation of Hexagonal Boron Nitride and Titanium Dioxide Nanocomposite

2.2.1 Preparation and Exfoliation of Hexagonal Boron Nitride Nanosheets

The h-BNNs were prepared by a widely used physical method with controlled numbers of the layer. The 0.2 g h-BN (Sigma-Aldrich, American) powder was dispersed in a mixture of 100 ml of ethanol (Damao Chemical Reagent Factory, Tianjin, China) and 100 ml of deionized water, to prepare a large amount of stripped h-BNNs by mechanical ball milling.

2.2.2 Preparation of Hexagonal Boron Nitride and Titanium Dioxide Nanocomposite

The precursor of amorphous hydrate was prepared through the aqueous phase reaction of titanyl sulfate ($TiOSO_4$, Sigma-Aldrich, American) and 10% ammonium hydroxide solution ($NH_3{\cdot}H_2O$, Damao Chemical Reagent Factory, Tianjin, China) in an ice bath until a pH value of 6 is attained. The white precipitate was separated by centrifugation and washed with deionized water in three cycles to remove the sulfate ions. The fresh precipitate was mixed with a predefined volume of exfoliated h-BNNs suspension in water and subsequently refluxed at 80°C for 5 h to produce white precipitates. Using the method, samples of h-BN-TiO_2 nanocomposite were prepared.

2.3 Characterization of Hexagonal Boron Nitride and Titanium Dioxide Nanocomposite

The particle size and the morphology of the h-BN-TiO_2 nanocomposite were inspected using the transmission electron microscope (TEM, Tecnai F30, FEI, Hillsboro, American) and the atomic force microscope (AFM, Multimode 8-HR, BRUKER, American). The crystal structure of the h-BN-TiO_2 nanocomposite was characterized by X-Ray diffraction (XRD, Smart APEX Ⅱ, BRUKER, German) patterns and the Raman spectra were measured using the micro confocal Raman spectrometer (LabRAM HR Evolution, HORIBA Jobin Yvon S.A.S, Paris, France) with 532 nm laser excitation.

2.4 Preparation of Hexagonal Boron Nitride and Titanium Dioxide/Glass Ionomer Cement Composite

Commercial GIC (Chang Shu Shang Chi Dental Materials, Chang Shu, China) was selected for this study. The powder are composed of silica (SiO_2), CaF_2, sodium fluorosilicate (Na_2SiF_6), aluminum oxide (Al_2O_3), and aluminium phosphate ($AlPO_4$); the liquid are composed of polyacrylic acid, tartaric acid, and deionized water. The prepared h-BN-TiO_2 and GIC powders were weighed when the ratio of h-BN-TiO_2 to the GIC powder was 0, 0.3, 0.7, 1.1, 1.5 wt%, respectively. The quantitative h-BN-TiO_2/GIC powder and GIC liquid were mixed on a ratio of 2:1. The mixture was thoroughly shaken and quickly transferred to the mold for compression, after it was formed and the sample was stored at 100% relative humidity at 37°C for 24 h.

2.5 Characterization of Hexagonal Boron Nitride and Titanium Dioxide/Glass Ionomer Cement Composites

2.5.1 Mechanical Performance Test of Hexagonal Boron Nitride and Titanium Dioxide/Glass Ionomer Cement Composites

2.5.1.1 Vicker Hardness Test

The VHN test was conducted on each group of 5 specimens with a diameter and thickness of 10 mm and about 5 mm, respectively using a Vicker Hardness Tester (HV-1000IS, SIOMN, Shanghai, China) with a load of 100 g and a dwelling time of 10 s, and the average results were analyzed. The diagonal length of each indentation was measured directly using a graduated eyeglass Lens. The VHN was obtained using the following Formula 5:

$$VHN = \frac{0.1891F}{d^2}$$

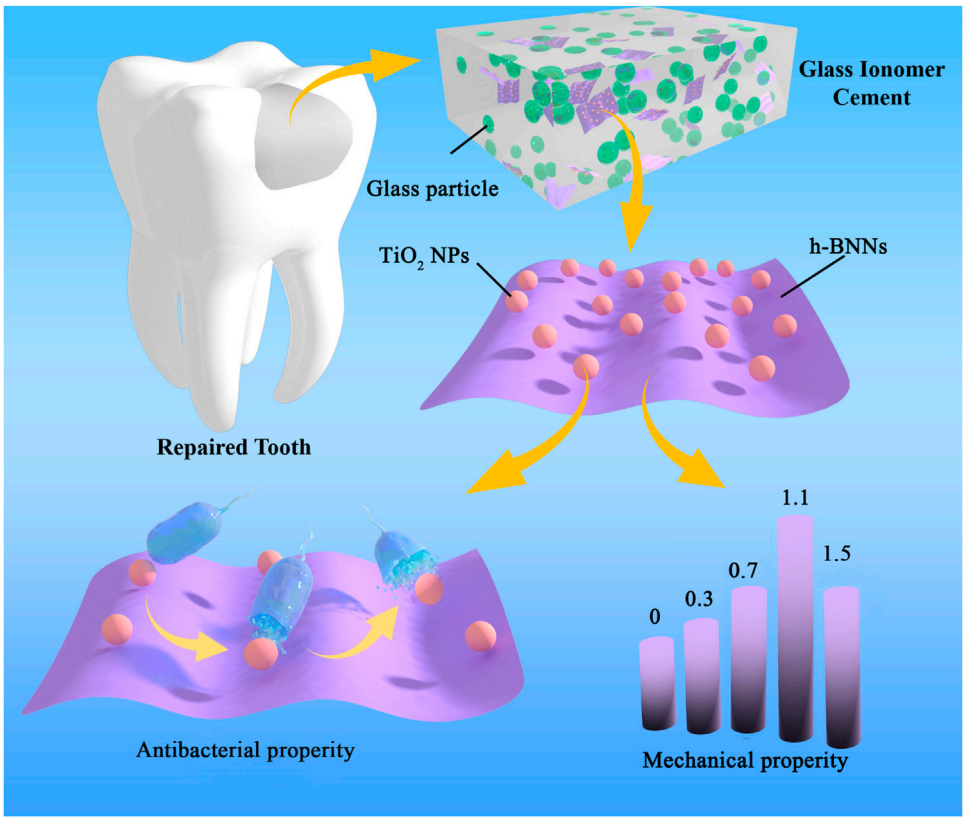

FIGURE 1 | Schematic diagram of synthesis and performance evaluation h-BN-TiO_2/GIC composites.

Where d is the length of the diagonals (mm) and F denotes the load (N).

2.5.1.2 Cs Test

A cylinder (4 mm in diameter, 6 mm in high) made from quartz glass molds was the compression specimen. The CS test was performed on a universal testing machine (312 Frame, Test Resources, United States) at a rate of 0.5 mm/min (Sun et al., 2018). The CS was calculated based on the following formula:

$$CS = \frac{F}{r^2}$$

where F is the load at the fracture point (N) and r denotes the radius of the cylindrical specimen (mm).

2.5.1.3 Friction Experiment

Three samples of each ratio (10 × 4 × 6 mm) were prepared and cured for 24 h. Zirconia ceramic balls with a diameter of 6 mm were selected for testing on the UMT-2 friction testing machine (UMT-2, CETR, American). The experimental parameters are set as follows: the loading force, speed, frequency, test time, and the running distance of the sample were 5 N, 10 mm/s, 2 Hz, 20 min, and 5 mm, respectively (Sun et al., 2018). The COF was automatically calculated by computer software.

2.5.2 Scanning Electron Microscope Observation

To evaluate the morphology of the materials, the scanning electron microscope (SEM, Nova200 NanoLab, FEI, Eindhoven, Nederlanden) was used to analyze the fractured surfaces of pure GIC and h-BN-TiO_2/GIC composites.

2.5.3 Evaluation of Solubility

Five specimens were prepared for each group and immersed in artificial saliva at 37°C. The samples were taken out after 1, 7, 14, 28, and 35 days, respectively, and the surface was rinsed with deionized water. After drying, the comparison of the weights before and after immersing in artificial saliva were done to calculate solubility of per sample weight. The associated calculations were presented in the following equation:

$$S = \frac{M_0 - M_1}{M_0}$$

where M_1 denotes the weight of the soaked sample after x days (1 = 1, 7, 14, 28, 35), M_0 is the row weight of the specimen.

2.5.4 Evaluation of Biological Performance

2.5.4.1 Direct Contact Test

The DCT method (Sun et al., 2018) was used to evaluate the h-BN-TiO_2/GIC composites against *Streptococcus mutans* (*S. mutans*, ATCC®700610). Round samples and glass slides with a diameter

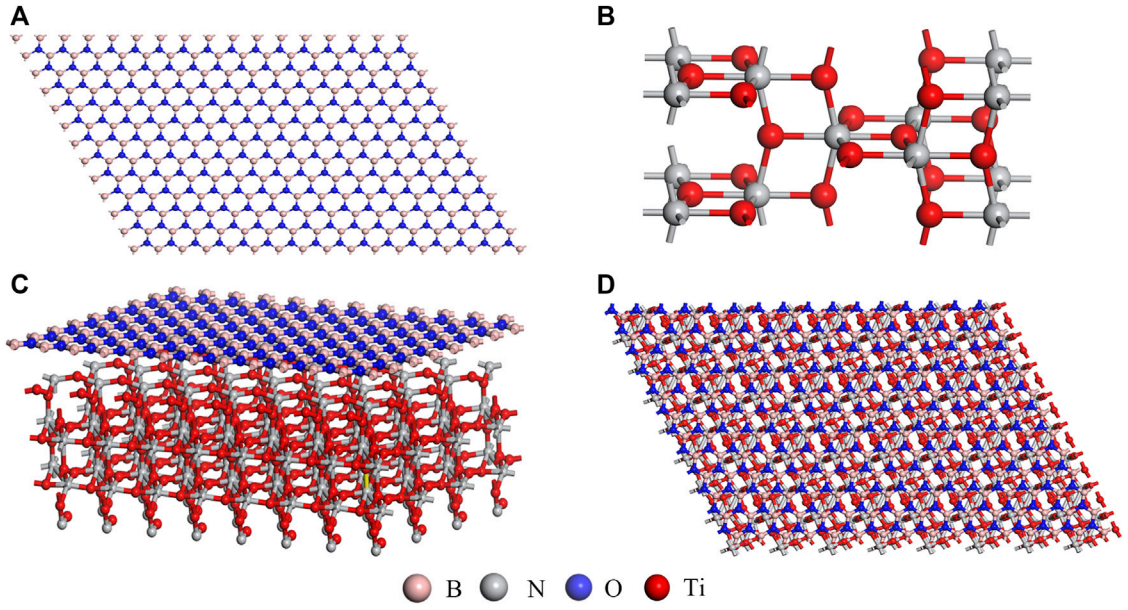

FIGURE 2 | Heterostructures of h-BN and TiO_2 **(A,B)**, h-BN-TiO_2 side views **(C)** and top views **(D)**.

of 10 mm were prepared, cleaned and disinfected with 75% alcohol. Then 100 μL bacterial suspension with a concentration of 10^6 CFU/ml was drawn and dropped onto the sample surface until the glass slide was covered. After incubation in a biochemical incubator (SHP-150PY, Jing hong, Shanghai) for 24 h, the sample and the surface of the slides were washed with PBS; Subsequently, the washing solution was diluted 100 times for the plating test and the analysis of the data. The measurement was replicated thrice in each group, and the loss of viability (VL) in the S.mutans was calculated as follows:

$$V_L = \frac{N_m - N_x}{N_x} 100\%$$

where N_m denotes the numbers of colonies corresponding to the blank group and N_x (x = 0, 0.3, 0.7, 1.1, 1.5) corresponds to the h-BN-TiO_2/GIC (0 wt%), h-BN-TiO_2/GIC (0.3 wt%), h-BN-TiO_2/GIC (0.7 wt%), h-BN-TiO_2/GIC (1.1 wt%) and h-BN-TiO_2/GIC (1.5 wt%) composites, respectively.

2.5.4.2 Scanning Electron Microscope Observation

The sample preparation method was the same as above. The disinfected h-BN-TiO_2/GIC specimen was placed in the pore cell culture plate, *S.mutans* suspension was added and subsequently incubated in a biochemical incubator for 4 h. After fixing in 2.5% glutaraldehyde (Sigma-Aldrich, American) and dehydrated in graded ethanol, the sample was observed using SEM after spraying with gold.

2.5.4.3 Cytotoxicity Testing

The cytotoxicity of the sample was detected through the evaluation of the effect of the sample on the viability and morphology of mouse fibroblasts (L-929, Shanghai Cell Bank, Chinese Academy of Sciences) *in vitro*. The sample preparation and sterilization methods were the same as before. Based on ISO standard, the extract was prepared with DMEM serum-free (Sigma-Aldrich, American) cell culture medium with a specific surface area/volume ratio of 3 cm^2/ml, and the eluate was prepared by incubating for 24 h in a biochemical incubator. The cells were seeded in a 96-well cell culture plate at a cell culture medium concentration of 5×10^3/(100 μl) per well and adhered to the wall after 24 h of culture. Subsequently, the medium is replaced with 100 μl of sample eluate and with the addition of 10 μl of tetramethylammonium salt (MTT tetrazolium salt; Sigma-Aldrich, American) to each well. The incubation period is continued for 24, 48, and 72 h in a biochemical incubator, and absorbance was measured at 490 nm using the enzyme-labeled method. The experiment was replicated thrice.

2.6 Statistical Analysis

All statistical analysis were conducted using GraphPad Prism (V6.01, GraphPad Software, San Diego, CA, United States) and Origin (2019, Origin Lab, Northampton, Massachusetts, United States) Windows version. Tukey's test was used in the subsequent multiple comparisons, the difference was considered significant when $p < 0.05$, and the difference was very significant when $p < 0.001$. All determinations were independently replicated thrice to ensure reproducibility.

3 RESULTS

3.1 Characterization of Hexagonal Boron Nitride and Titanium Dioxide Nanocomposite

The MD simulations of the adsorption of TiO_2 onto the h-BN are shown in **Figure 2**. There refer to the molecular models of h-BN (**Figure 2A**) and TiO_2 (**Figure 2B**) after structural optimization.

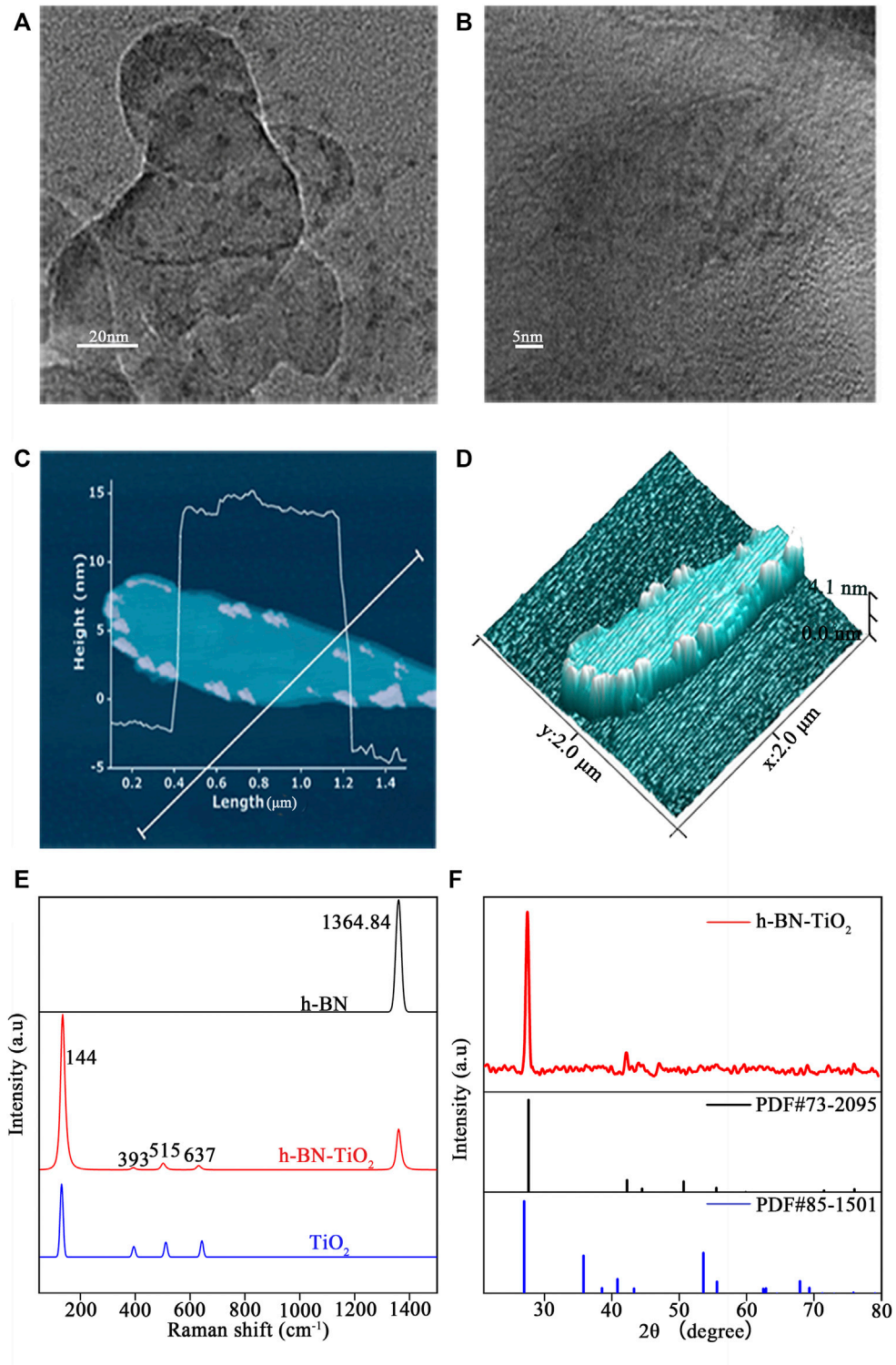

FIGURE 3 | TEM analysis of h-BN-TiO_2 by low **(A)** and high **(B)** magnification images. And the prepared h-BN-TiO_2 **(C,D)** were observed by AFM. Raman spectrometry **(E)** and XRD patterns **(F)** of prepared h-BN-TiO_2.

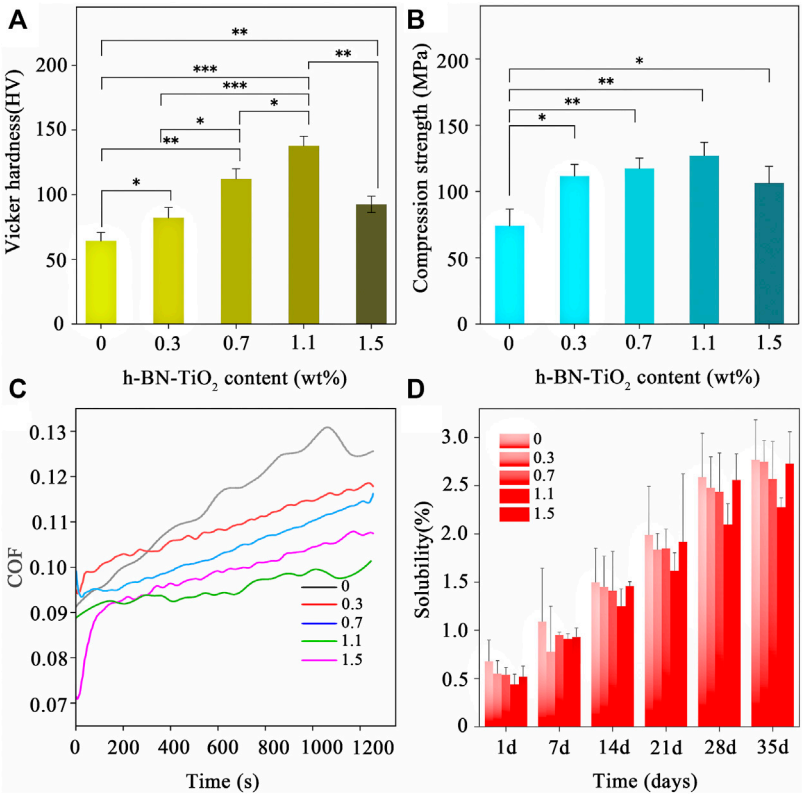

FIGURE 4 | Mechanical properties and solubility of h-BN-TiO_2/GIC composite (0, 0.3, 0.7, 1.1, 1.5 wt%). **(A)** Vicker hardness (in HV); **(B)** Compression stress (in MPa); **(C)** the real-time COF; and **(D)** solubility (%).

Figures 2C,D show the final XSD structure of the TiO_2 and the h-BN from the MD simulations. It was found by calculation that the adsorption energy of TiO_2 onto the surface of h-BN was −235 kcal/mol, indicating that the adsorption process was exothermic.

The morphologies of the h-BNNs and TiO_2 NPs were observed by TEM. **Figure 3A** shows that the h-BN featured a thin and transparent two-dimensional nanostructure with a lateral dimension ranging from 200 nm to 1 μm, while the TiO_2 NPs exhibited diameters ranging from ranging from 20 to 200 nm after growing *in situ* on the surface of the h-BNNs. The lattice fringes of the TiO_2 NPs were observed under high magnification (**Figure 3B**). To further investigate the unique structure of the h-BN-TiO_2 nanocomposite, AFM was used to observe the three-dimensional morphology. **Figure 3C** shows that the h-BNNs and TiO_2 NPs form a rivet structure with a minimum thickness of 4.0 nm (**Figure 3D**). In addition, the Raman spectrum confirmed the existence of an h-BN-TiO_2 nanocomposite (**Figure 3E**). In previous studies, the Raman spectra of h-BNNs featured peaks near 1,364.84 cm^{-1} (Czarniewska et al., 2019), and anatase TiO_2 NPs peaks were located at 144 cm^{-1} (Eg1), 197 cm^{-1} (Eg2), 393 cm^{-1} (B1g), 512 cm^{-1} (B1g + A1g), and 635 cm^{-1} (Eg3) (Choi et al., 2005), all of which were consistent with the peaks in the Raman spectrum of the h-BN-TiO_2 nanocomposite in this study. In addition, the XRD patterns of h-BN-TiO_2 nanocomposite are shown in **Figure 3F**. All these diffraction peaks match well with the standard values of h-BN (PDF#73-2095) and TiO_2 (PDF#85-1501) and were highly consistent with the Raman spectroscopy results.

3.2 Mechanical Properties of the Hexagonal Boron Nitride and Titanium Dioxide/Glass Ionomer Cement Composites

Figures 4A,B show the VHN and CS results of the h-BN-TiO_2/GIC with 0, 0.3, 0.7, 1.1, and 1.5 wt% loading of the h-BN-TiO_2 nanocomposite. Compared to the 0 wt% h-BN-TiO_2/GIC composite, the CS of the h-BN-TiO_2/GIC composite (0.3, 0.7, 1.1, 1.5 wt%) increased by 32.8%, 64.5%, 80.2%, and 52.6%, respectively, while the VHN increased by 25.6%, 77.9%, 149.65%, and 56.5%, respectively. The VHN and CS of the 1.1 wt% h-BN-TiO_2 were the highest of all the nanocomposites, while the values began to decline from 1.5 wt%. The VHN and CS of the 1.1 wt% h-BN-TiO_2/GIC were 149.65% and 80.2% higher than the 0 wt% h-BN-TiO_2/GIC ($p < 0.001$).

Next, the friction performance of the nanocomposites were assessed. The changes in the coefficient of friction (COF) of the h-BN-TiO_2/GIC composites over time were shown in **Figure 4C**. The COF of the h-BN-TiO_2/GIC composites were more stable throughout the friction tests, and the friction curves generated from the data were smooth without fluctuations. The COF of the h-BN-TiO_2/GIC composite (0.3, 0.7, 1.1, 1.5 wt%) were lower

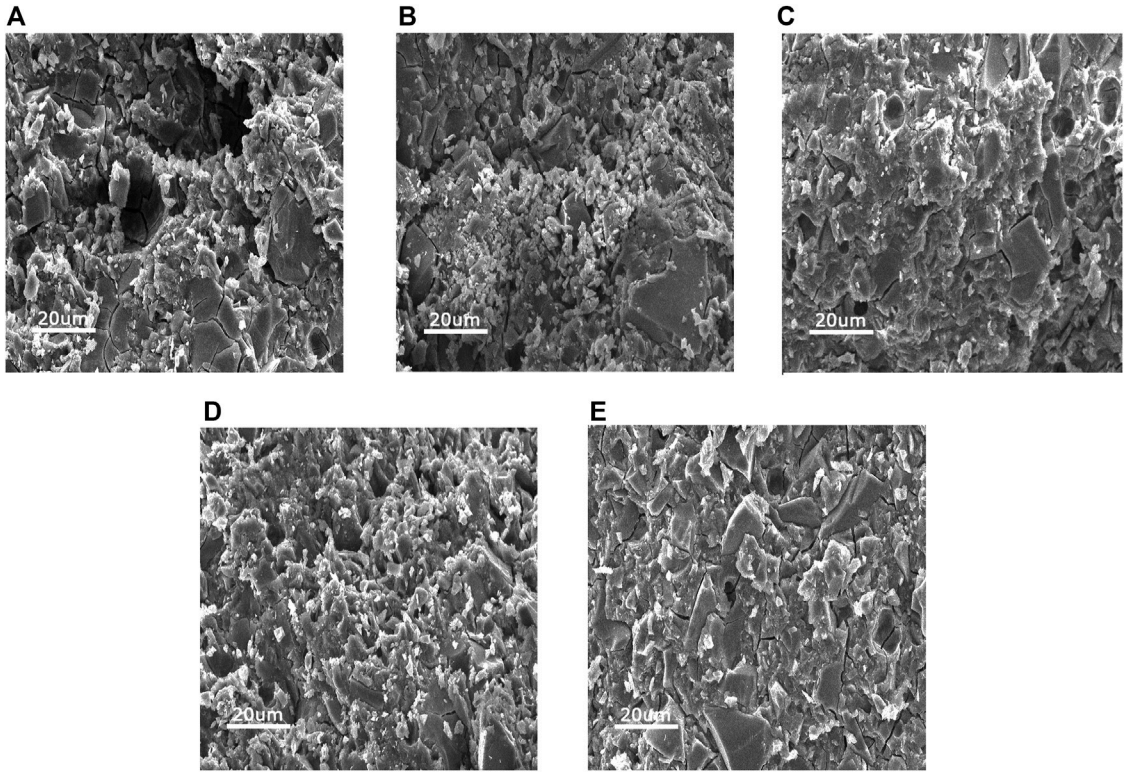

FIGURE 5 | The SEM images of the fractured surfaces of h-BN-TiO_2/GIC composites after the compression test with h-BN-TiO_2 nanocomposite concentration of **(A)** 0 wt%, **(B)** 0.3 wt%, **(C)** 0.7 wt%, **(D)** 1.1 wt%, **(E)** 1.5 wt%.

than the 0 wt% h-BN-TiO_2/GIC starting from 380 s, with the 1.1 wt% h-BN-TiO_2/GIC exhibiting the highest friction resistance.

3.3 Solubility of Hexagonal Boron Nitride and Titanium Dioxide/Glass Ionomer Cement Composites

Figure 4D shows the average solubilities of the h-BN-TiO_2/GIC (0, 0.3, 0.7, 1.1, 1.5 wt%) composites on days 1, 7, 14, 21, 28, and 35. The figures showed that the solubility of pure GIC was higher than the solubilities of the GIC composites on each day. During the first day of the solubility experiments, there were no significant differences among the h-BN-TiO_2/GIC composite groups. However, lower solubilities of the nanocomposite were manifested after extending the soaking duration and increasing the amount of h-BN-TiO_2. The 0.7 wt% and 1.1 wt% h-BN-TiO_2/GIC composites exhibited the lowest solubilities after day 14.

3.4 Characterization of the Prepared Hexagonal Boron Nitride and Titanium Dioxide/Glass Ionomer Cement Composites

SEM images of the h-BN-TiO_2/GIC (0, 0.3, 0.7, 1.1, 1.5 wt%) composites were acquired after undergoing compressive strength tests at low magnification (×500, **Figure 5**). The h-BN-TiO_2 nanocomposite was found to be uniformly dispersed throughout the GIC but could easily be distinguished from the GIC material. Some cracks and pores were observed on the fracture surfaces of all samples, but only a few of these structures were observed in the pure GIC without h-BN-TiO_2 nanocomposite.

3.5 Evaluation of Biological Performance

Figure 6(A–F) displays the antibacterial efficacy of the h-BN-TiO_2/GIC composites (0, 0.3, 0.7, 1.1, 1.5 wt%). Although the GIC had a certain degree of antibacterial effect, the h-BN-TiO_2/GIC composites (0.3, 0.7, 1.1, 1.5 wt%) showed a stronger antibacterial effect. Compared with the blank non-bacterial samples, the antibacterial rates of h-BN-TiO_2/GIC composites (0.3, 0.7, 1.1, 1.5 wt%) were 14.5%, 38.4%, 67.2%, 93.4%, and 76.9%, respectively (**Figure 7C**). Based on the loss of viability of *S.mutans* in the GIC composites containing different concentrations of the h-BN-TiO_2 nanocomposite, we find the nanocomposites had a better antibacterial effect than pure GIC without h-BN-TiO_2 nanocomposite.

The *S. mutans* adhered to and aggregated on the surface of the GIC after 4 h of incubation and SEM images were obtained. **Figures 7A,D** (magnification ×3,000) and **Figures 7B,E** (magnification ×5,000) represented the 0 wt% and 1.1 wt% h-BN-TiO_2/GIC composites, respectively. 1.1 wt% the h-BN-TiO_2/GIC composite

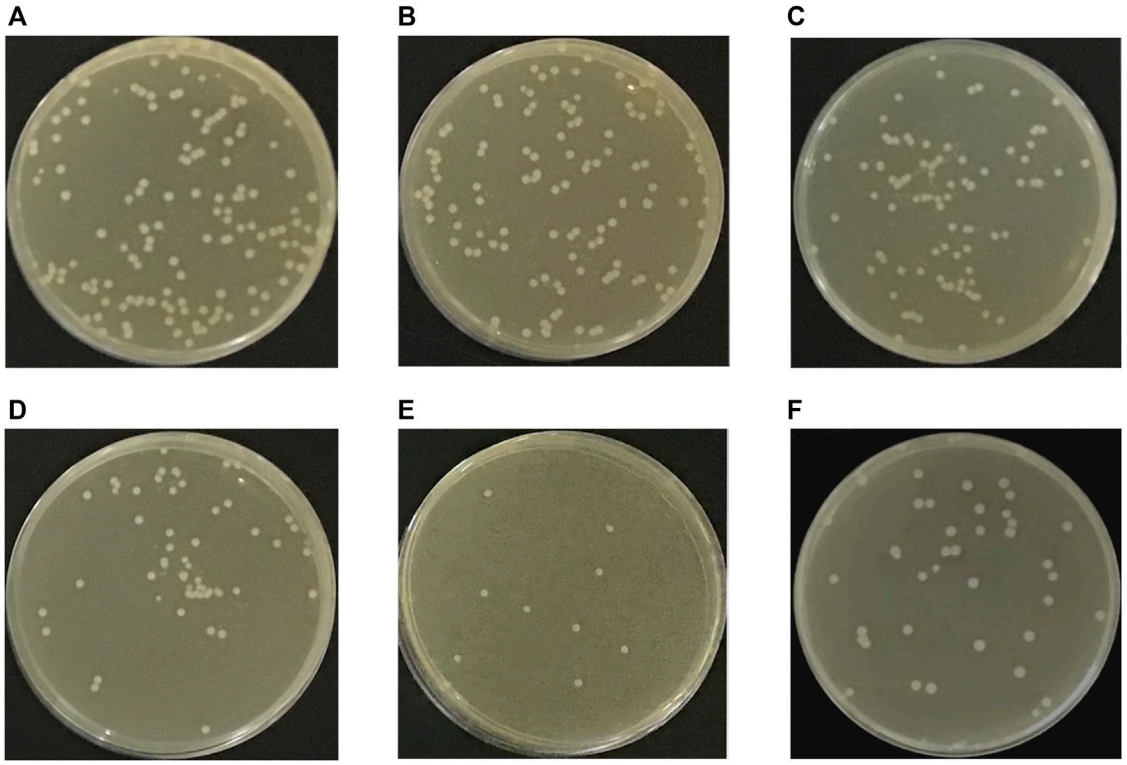

FIGURE 6 | *S. mutans* colonies on agar of blank group **(A)**, h-BN-TiO_2/GIC (0 wt%) and h-BN-TiO_2/GIC (0.3 wt%), h-BN-TiO_2/GIC (0.7 wt%), h-BN-TiO_2/GIC (1.1 wt%), h-BN-TiO_2/GIC (1.5 wt%) composites **(B–F)**, respectively.

shows that the number of viable bacteria substantially decreased and the morphologies of bacteria damaged compared with 0 wt% h-BN-TiO_2/GIC composite.

The extent of cell damage by the nanocomposite was evaluated using MTT assays at while culturing the bacteria for 24, 48, and 72 h (**Figure 7F**). After co-culturing the cell strain L929 and the extracts of h-BN-TiO_2/GIC composite, the cell viability of 0 wt% h-BN-TiO_2/GIC reached up to 70% at 24 h. Although the h-BN-TiO_2/GIC composites (0.3, 0.7, 1.1, 1.5 wt%) had lower viability at 24 h, the cell viability also increased after 48 and 72 h. The nanocomposites did not significant affect the viability of the L929 cells ($p > 0.5$), indicating that the h-BN-TiO_2/GIC composites were biologically compatible.

4 DISCUSSION

The poor mechanical and antibacterial properties of traditional GIC limit the utility of this restorative material in clinical applications. However, the addition of nanomaterials into the GIC matrix as dispersion enhancers have the potential to significantly improve the respective performances of traditional GIC.

In this study, h-BNNs were combined with TiO_2 NPs to obtain a zero-dimensional-two-dimensional nanocomposite system, after which we theoretically studied the mechanism of formation of the GIC composites comprising the h-BNNs and TiO_2 nanocomposite, with emphasis on the impact of the h-BN-TiO_2 nanocomposite on the performance of the GIC. The theoretical and experimental results both established that, although a two-dimensional structure similar to graphene was formed, the delocalization of the electrons throughout the h-BN were completely different compared to graphene. The h-BN prepared by the ball-milling was negatively charged (Fu et al., 2013), and the surface charge of the TiO_2 NPs depended on the pH value of the solution. In an acidic medium, the surface of the TiO_2 NPs is positively charged (Hoffmann et al., 1995); therefore, the positive charge of the surface of the TiO_2 NPs enabled the stable formation of a h-BN-TiO_2 nanocomposite structure with the negatively charged h-BN monolayer through electrostatic interactions in this work. In addition, mechanical cutting forces caused the thin, multilayered h-BNNs to separate into single h-BN layers, creating a structural basis for the cohesiveness between the TiO_2 NPs and h-BNNs, which is also important for enhancing the electrostatic attraction. The adsorption energy of the TiO_2 NPs onto the h-BNNs in the h-BN-TiO_2 composite was calculated to be −235 kcal/mol through MD simulations. This negative adsorption energy indicated that the two-dimensional-zero-dimensional heterostructure had a lower energy and a more stable configuration, implying that the experimental preparation of the nanocomposite resulted in a reduction in entropy. Therefore, this method could be used for the effective preparation of the h-BN-TiO_2 nanocomposite.

The h-BN-TiO_2 nanocomposite was prepared using ball-milling and thermal hydrolysis methods. TEM and AFM images showed that the h-BN-TiO_2 nanocomposite exhibited a rivet-like

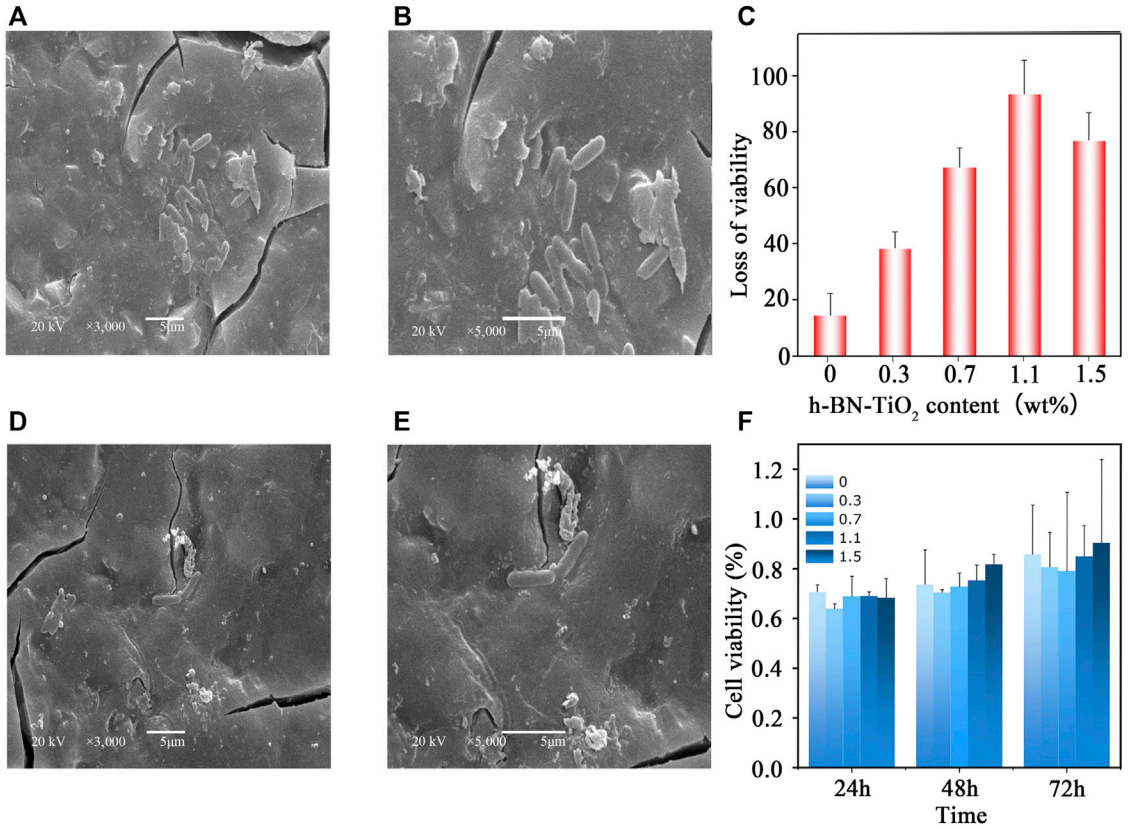

FIGURE 7 | The SEM micrograph of the colony of representative samples from the groups of h-BN-TiO_2/GIC: 0 wt% h-BN-TiO_2/GIC **(A)** magnification ×3,000; 0 wt.%h-BN-TiO_2/GIC **(B)**, magnification ×5,000; 1.1 wt.%h-BN-TiO_2/GIC **(D)**, magnification ×3,000; 1.1 wt.%h-BN-TiO_2/GIC **(E)**, magnification ×5,000; The influence of different concentrations of the h-BN-TiO_2/GIC composites on the loss of viability in *S. mutans* **(C)** and the cell viability of the L-929 cells cultured in h-BN-TiO_2/GIC extract **(F)**.

structure composed of two-dimensional nanosheets with thicknesses of 200 nm–1 μm and zero-dimensional nanoparticles with diameters of 20–200 nm. In addition to the prevention of the agglomeration of the h-BNNs, SEM confirmed not only the rivet-like structure of the h-BN-TiO_2 nanocomposite but also that the h-BN-TiO_2 nanocomposite were uniformly dispersed throughout the GIC matrix. Furthermore, significant improvements in the CS and VHN of the h-BN-TiO_2/GIC composite compared to the traditional GIC were observed, which indicated that the h-BN-TiO_2 nanocomposite had a significant impact on the mechanical properties of GIC. Compared to the GIC without the h-BN-TiO_2 nanocomposite (0 wt% h-BN-TiO_2/GIC), the VHN and CS of the 1.1 wt% h-BN-TiO_2/GIC increased by 149.65% and 80.2%, respectively, which were the highest of all of the h-BN-TiO_2/GIC composites; furthermore, the CS and VHN values decreased as the concentration of the h-BN-TiO_2 in the composite increased to 1.5 wt%.

There were three potential mechanisms by which h-BN-TiO_2 nanocomposite enhanced the performance of the GIC substrate. First, because the ultra-thin h-BN-TiO_2 nanocomposite was evenly dispersed in the GIC matrix, when the composite was subjected to external stress, the rigid nanosheets effectively functioned as conductors for the external stress, resulting in the reinforcement of the composite. Second, the discrete rivet-like structures of the TiO_2 NPs were tightly embedded within the thin layer of the h-BNNs by adsorption manifested by electrostatic interactions; when subjected to external stress, the TiO_2 NPs distributed throughout the surface of the h-BNNs not only effectively dissipated the stress but also prevented excessive external stress from removing the h-BNNs from the substrate, thereby enhancing the mechanical strength of the GIC substrate. Third, there was a good combination between TiO_2 NPs as additional polyacrylic polymer attachment sites and the GIC matrix; therefore, when the TiO_2 NPs were removed from the GIC matrix by external stress, a large amount of local stress needed to be dissipated to effectively strengthen the GIC. However, when the concentration of the h-BN-TiO_2 nanocomposite was higher than 1.1 wt%, the nanomaterials tended to have lower surface energies, making it easier for them to combine *via* van der Waals forces. The agglomeration of the materials decreased their surface energy until reaching a stable energy, making it impossible to effectively achieve uniform dispersion throughout the GIC. The agglomerated nanocomposites became a significant source of defects that manifested concentrated local stresses in the GIC. When subjected to external stress, the GIC first broke from the stress concentration; therefore, the defects caused by the agglomeration reduced the mechanical strength of the GIC.

This study also evaluated the effects of the concentration of the h-BN-TiO_2 nanocomposite on the friction coefficient of the GIC. As the amount of h-BN-TiO_2 nanocomposite was increased, the COF of GIC composites became decrease. The nanomaterial containing 1.1 wt% of the h-BN-TiO_2/GIC composite had the lowest wear coefficient, confirming that the h-BN-TiO_2 nanocomposite improved the wear resistance of GIC. Also, the addition of the h-BNNs into simultaneously enhanced the stiffness and toughness of the GIC matrix, thereby preventing the GIC matrix from propagating along cracks caused by friction. Furthermore, the addition of the h-BN-TiO_2 nanocomposite into the GIC matrix reduced the distance between the particles and effectively protected the matrix, thereby reducing the incidence of peeling and improving the overall wear resistance of the material. Since the friction experiments were mainly performed on the surfaces of the samples, and the results obtained were consistent with the surface hardness trends, we speculated that the increase in surface hardness might potentially be the cause of the increased friction performance.

Solubility is an important factor affecting the mechanical and antibacterial properties of dental materials. The GIC surface gradually erodes after being in contact with various liquids, resulting in the dissolution of the chemical components of the matrix. Importantly, GIC has a high dissolution rate during the initial curing period (Brito et al., 2010). The main reason for this is that, during the curing process, the anions within the GIC matrix can interact with sodium ions to form soluble compounds, resulting in continuous dissolution. However, we found that the solubility of GIC composites gradually decreased as the concentration of the h-BN-TiO_2 nanocomposite increased, likely because the addition of the h-BN-TiO_2 nanocomposite reduced the internal pores of the GIC, and they acted as a micro-separator, causing the material to form a porous structure, which subsequently increased the stability of the GIC matrix and reduced its dissolution rate. As we all know, environmental humidity and water absorption have a significant impact on the mechanical properties of materials (Randhawa and Patel, 2021), especially in the oral environment for dental materials. However, due to the limitations of experimental conditions in this study, the water absorption and ambient humidity are not discussed, which is also one of the limitations of in the paper. It is well-known that traditional GIC has fluoride-releasing properties, but the fluoride-releasing capacity of GIC in the oral cavity is the highest within the first two months of implantation, after which it gradually decreases (Sidhu and Nicholson, 2016). Although, GIC can absorb free fluoride ions in the oral cavity and store them for later release (Hasan et al., 2019). However, these trace amounts of fluoride ions are not enough to inhibit the formation of biofilms. In addition to being highly biocompatible, the 1.1 wt% h-BN-TiO_2/GIC composite we developed effectively killed 93.4% of the total S.mutans bacteria. SEM observation of the bacteria morphology after conducting the antibacterial efficacy experiments revealed that the GIC composites compromised the integrity of the bacteria cell membranes, which was evident because the bacteria exhibited a pronounced ruffled appearance. This result was mainly attributed to the synergistic antibacterial effect of the h-BN-TiO_2 nanocomposite. The antibacterial properties of the nanocomposite were derived from two different mechanisms. First, the sharp edges of the boron nitride nanosheets caused mechanical damage to the bacterial cell membrane, causing cell deformation and lysis. Second, the electrostatic effect between the positively charged TiO_2 NPs and the negatively charged cell membrane disrupted the inherent functions of the bacterial cell membrane (Sondi and Salopek-Sondi, 2004; Devanesan and AlSalhi, 2021), leading to the eventual death of the bacteria. In this study, we only tested the antibacterial effects of the h-BN-TiO_2/GIC composites over 24 h; thus, the long-term antibacterial effects of the composites and its effect on the occurrence of secondary caries need to be further studied. Another limitation of this study involves the lack of understanding of the long-term aging performance of the h-BN-TiO_2/GIC composite. Therefore, it is necessary to further explore the long-term effects of the h-BN-TiO_2/GIC composites to ensure the viability of its clinical application.

5 CONCLUSION

In this study, we successfully prepared a two-dimensional-zero-position nanocomposite system composed of h-BNNs and TiO_2 NPs and simulated the formation of the composite from the h-BN and TiO_2 components at the atomic scale using MD simulations. The combination of the h-BN-TiO_2 nanocomposite with the GIC was enabled through electrostatic forces, and the nanocomposite particles were uniformly dispersed throughout the GIC matrix. Moreover, the addition of 1.1 wt% of the Compressive strength (CS), Vicker hardness (VHN) and antibacterial properties were 80.2%, 149.65%, and 93.4% higher, respectively. The increase in the concentration of the h-BN-TiO_2 nanocomposite led to a decrease in both the frictional coefficient and solubility. In addition, the material exhibited excellent biocompatibility and satisfied the biomedical requirements. Thus, this study provided a novel method for enhancing the performance of GIC.

Further studies are required to investigate the long-term aging performance of the h-BN-TiO_2/GIC composites and water absorption. Also, different test conditions can be selected to test the effect of environmental conditions on the properties of h-BN-TiO_2/GIC composite.

DATA AVAILABILITY STATEMENT

The original contributions presented in the study are included in the article/**Supplementary Material**, further inquiries can be directed to the corresponding authors.

AUTHOR CONTRIBUTIONS

YM, BL, and X-JH conceived this study; Y-ZG, J-CY, and H-LJ conducted sample preparation and testing of all samples; Y-RW performed the theoretical calculations; YL conducted cell experiments and analyzed the data; X-ZK, R-ZL, Q-ZH, and C-DZ analyzed part data; YM and Y-ZG wrote the manuscript.

FUNDING

This work also supported by the Fundamental Research Funds for the Central Universities (lzujbky-2020-52) and the Research Fund of Lanzhou University School/Hospital of Stomatology (lzukqky-2021-q02). The authors are grateful to Lanzhou Hand and Foot Surgery Hospital for financial support.

ACKNOWLEDGMENTS

The authors thank the National Natural Science Foundation of China (No. 81970976), the Natural Science Foundation of Gansu Province (20JR10RA593) and Science and Technology Planning Project of Chengguan District, Lanzhou City (2021-2-1) for support. All the authors thank the Clinical Research Center of Shanxi Province for Dental and Maxillofacial Diseases (2020YHJB04), College of Stomatology, Xi'an Jiaotong University. The authors are grateful to the Michigan Center for Materials Characterization (MC)2 for its assistance with electron microscopy used in this work.

SUPPLEMENTARY MATERIAL

The Supplementary Material for this article can be found online at: https://www.frontiersin.org/articles/10.3389/fmats.2022.883027/full#supplementary-material

REFERENCES

Abdallah, R. M., Abdelghany, A. M., and Aref, N. S. (2020). Does Modification of Amalgomer with Propolis Alter its Physicomechanical Properties? an *In Vitro* Study. *Int. J. Biomater.* 2020, 1–10. doi:10.1155/2020/3180879

Brito, C. R., Velasco, L. G., Bonini, G. A. V. C., Imparato, J. C. P., and Raggio, D. P. (2010). Glass Ionomer Cement Hardness after Different Materials for Surface Protection. *J. Biomed. Mater. Res.* 93 (1), 243-246. doi:10.1002/jbm.a.32524

Chen, B., Jiang, Y., Zhao, M., Wang, W., Chu, Z., Huo, R., et al. (2020). Ag Nanoparticles Decorated Hybrid Microspheres for Superior Antibacterial Properties. *Mater. Lett.* 262, 127057. doi:10.1016/j.matlet.2019.127057

Ching, H. S., Luddin, N., Kannan, T. P., Ab Rahman, I., and Abdul Ghani, N. R. N. (2018). Modification of Glass Ionomer Cements on Their Physical-Mechanical and Antimicrobial Properties. *J. Esthet Restor Dent* 30 (6), 557–571. doi:10.1111/jerd.12413

Choi, H. C., Jung, Y. M., and Kim, S. B. (2005). Size Effects in the Raman Spectra of TiO2 Nanoparticles. *Vibrational Spectrosc.* 37 (1), 33–38. doi:10.1016/j.vibspec.2004.05.006

Czarniewska, E., Mrówczyńska, L., Jędrzejczak-Silicka, M., Nowicki, P., Trukawka, M., and Mijowska, E. (2019). Non-Cytotoxic Hydroxyl-Functionalized Exfoliated Boron Nitride Nanoflakes Impair the Immunological Function of Insect Haemocytes *In Vivo*. *Sci. Rep.* 9 (1), 14027. doi:10.1038/s41598-019-50097-0

Devanesan, S., and AlSalhi, M. S. (2021). Green Synthesis of Silver Nanoparticles Using the Flower Extract of Abelmoschus Esculentus for Cytotoxicity and Antimicrobial Studies. *Int. J. Nanomedicine* 16, 3343–3356. doi:10.2147/IJN.S307676

Elsaka, S. E., Hamouda, I. M., and Swain, M. V. (2011). Titanium Dioxide Nanoparticles Addition to a Conventional Glass-Ionomer Restorative: Influence on Physical and Antibacterial Properties. *J. Dent* 39 (9), 589–598. doi:10.1016/j.jdent.2011.05.006

Farooq, M. U., Jan, R., Azeem, M., Umer, M. A., Akram, M. A., Khan, A. N., et al. (2020). Enhanced Mechanical Properties of Functionalized BN Nanosheets-Polymer Composites. *J. Polym. Res.* 27 (10), 310. doi:10.1007/s10965-020-02286-z

Fu, X., Hu, Y., Yang, Y., Liu, W., and Chen, S. (2013). Ball Milled H-BN: An Efficient Holes Transfer Promoter to Enhance the Photocatalytic Performance of TiO2. *J. Hazard. Mater.* 244-245, 102–110. doi:10.1016/j.jhazmat.2012.11.033

Hajipour, M. J., Fromm, K. M., Akbar Ashkarran, A., Jimenez de Aberasturi, D., Larramendi, I. R. d., Rojo, T., et al. (2012). Antibacterial Properties of Nanoparticles. *Trends Biotechnol.* 30 (10), 499–511. doi:10.1016/j.tibtech.2012.06.004

Hamid, N., Telgi, R. L., Tirth, A., Tandon, V., Chandra, S., and Chaturvedi, R. K. (2019). Titanium Dioxide Nanoparticles and Cetylpyridinium Chloride Enriched Glass-Ionomer Restorative Cement: A Comparative Study Assessing Compressive Strength and Antibacterial Activity. *J. Clin. Pediatr. Dent* 43 (1), 42–45. doi:10.17796/1053-4625-43.1.8

Hasan, A. M. H. R., Sidhu, S. K., and Nicholson, J. W. (2019). Fluoride Release and Uptake in Enhanced Bioactivity Glass Ionomer Cement ("Glass Carbomer") Compared with Conventional and Resin-Modified Glass Ionomer Cements. *J. Appl. Oral Sci.* 27, e20180230. doi:10.1590/1678-7757-2018-0230

Hoffmann, M. R., Martin, S. T., Choi, W., and Bahnemann, D. W. (1995). Environmental Applications of Semiconductor Photocatalysis. *Chem. Rev.* 95 (1), 69–96. doi:10.1021/cr00033a004

Lee, B., Kwon, J.-S., Khalid, M. W., Kim, K.-M., Kim, J., Lim, K. M., et al. (2020). Boron Nitride Nanoplatelets as Reinforcement Material for Dental Ceramics. *Dental Mater.* 36 (6), 744–754. doi:10.1016/j.dental.2020.03.002

Moheet, I. A., Luddin, N., Ab Rahman, I., Masudi, S. a. M., Kannan, T. P., and Abd Ghani, N. R. N. (2018). Evaluation of Mechanical Properties and Bond Strength of Nano-Hydroxyapatite-Silica Added Glass Ionomer Cement. *Ceramics Int.* 44 (8), 9899–9906. doi:10.1016/j.ceramint.2018.03.010

Moreau, J. L., and Xu, H. H. K. (2010). Fluoride Releasing Restorative Materials: Effects of pH on Mechanical Properties and Ion Release. *Dental Mater.* 26 (11), e227–e235. doi:10.1016/j.dental.2010.07.004

Moshaverinia, A., Ansari, S., Moshaverinia, M., Roohpour, N., Darr, J. A., and Rehman, I. (2008a). Effects of Incorporation of Hydroxyapatite and Fluoroapatite Nanobioceramics into Conventional Glass Ionomer Cements (GIC). *Acta Biomater.* 4 (2), 432–440. doi:10.1016/j.actbio.2007.07.011

Moshaverinia, A., Ansari, S., Movasaghi, Z., Billington, R. W., Darr, J. A., and Rehman, I. U. (2008b). Modification of Conventional Glass-Ionomer Cements with N-Vinylpyrrolidone Containing Polyacids, Nano-Hydroxy and Fluoroapatite to Improve Mechanical Properties. *Dental Mater.* 24 (10), 1381–1390. doi:10.1016/j.dental.2008.03.008

Moshaverinia, A., Roohpour, N., Billington, R. W., Darr, J. A., and Rehman, I. U. (2008c). Synthesis of N-Vinylpyrrolidone Modified Acrylic Acid Copolymer in Supercritical Fluids and its Application in Dental Glass-Ionomer Cements. *J. Mater. Sci. Mater. Med.* 19 (7), 2705–2711. doi:10.1007/s10856-008-3399-0

Moshaverinia, A., Roohpour, N., Darr, J. A., and Rehman, I. U. (2009a). Synthesis and Characterization of a Novel N-Vinylcaprolactam-Containing Acrylic Acid Terpolymer for Applications in Glass-Ionomer Dental Cements. *Acta Biomater.* 5 (6), 2101–2108. doi:10.1016/j.actbio.2009.02.015

Moshaverinia, A., Roohpour, N., and Rehman, I. (2009b). Synthesis and Characterization of a Novel Fast-Set Proline-Derivative-Containing Glass Ionomer Cement with Enhanced Mechanical Properties. *Acta Biomater.* 5 (1), 498–507. doi:10.1016/j.actbio.2008.06.011

Moshaverinia, M., Navas, A., Jahedmanesh, N., Shah, K. C., Moshaverinia, A., and Ansari, S. (2019). Comparative Evaluation of the Physical Properties of a Reinforced Glass Ionomer Dental Restorative Material. *The J. Prosthetic Dentistry* 122 (2), 154–159. doi:10.1016/j.prosdent.2019.03.012

Nicholson, J. W. (2016). Adhesion of Glass-Ionomer Cements to Teeth: A Review. *Int. J. Adhes. Adhesives* 69, 33–38. doi:10.1016/j.ijadhadh.2016.03.012

Nicholson, J. W., Braybrook, J. H., and Wasson, E. A. (1991). The Biocompatibility of Glass-Poly(alkenoate) (Glass-Ionomer) Cements: A Review. *J. Biomater. Sci. Polym. Edition* 2 (4), 277–285. doi:10.1163/156856291x00179

Nicholson, J. W., Sidhu, S. K., and Czarnecka, B. (2020). Enhancing the Mechanical Properties of Glass-Ionomer Dental Cements: A Review. *Materials* 13 (11), 2510. doi:10.3390/ma13112510

Randhawa, K. S., and Patel, A. D. (2020a). Enhancing Tribo-Mechanical Properties and thermal Stability of Nylon 6 by Hexagonal boron Nitride Fillers. *E-Polymers* 20 (1), 733–745. doi:10.1515/epoly-2020-0069

Randhawa, K. S., and Patel, A. D. (2020b). Influence of Boric Anhydride Reinforcement on Mechanical Properties and Abrasive Wear of Nylon 6. *Mater. Res. Express* 7 (5), 055303. doi:10.1088/2053-1591/ab8ee4

Randhawa, K. S., and Patel, A. D. (2020c). Tribological Behaviour of PA6/diborontrioxide Composites. *J. Phys. Conf. Ser.* 1706 (1), 012124. doi:10.1088/1742-6596/1706/1/012124

Randhawa, K. S., and Patel, A. (2021). The Effect of Environmental Humidity/Water Absorption on Tribo-Mechanical Performance of Polymers and Polymer Composites - a Review. *Ind. Lubrication Tribology* 73 (9), 1146–1158. doi:10.1108/ilt-02-2021-0045

Sidhu, S., and Nicholson, J. (2016). A Review of Glass-Ionomer Cements for Clinical Dentistry. *J. Funct. Biomater.* 7 (3), 16. doi:10.3390/jfb7030016

Simmons, J. J. (1990). Silver-Alloy Powder and Glass Ionomer Cement. *J. Am. Dent Assoc.* 120 (1), 49–52. doi:10.14219/jada.archive.1990.0018

Sondi, I., and Salopek-Sondi, B. (2004). Silver Nanoparticles as Antimicrobial Agent: A Case Study on *E. coli* as a Model for Gram-Negative Bacteria. *J. Colloid Interf. Sci* 275 (1), 177–182. doi:10.1016/j.jcis.2004.02.012

Sun, L., Yan, Z., Duan, Y., Zhang, J., and Liu, B. (2018). Improvement of the Mechanical, Tribological and Antibacterial Properties of Glass Ionomer Cements by Fluorinated Graphene. *Dental Mater.* 34 (6), e115–e127. doi:10.1016/j.dental.2018.02.006

Varela, M. F., Stephen, J., Lekshmi, M., Ojha, M., Wenzel, N., Sanford, L. M., et al. (2021). Bacterial Resistance to Antimicrobial Agents. *Antibiotics* 10 (5), 593. doi:10.3390/antibiotics10050593

Wang, S.-P., Ge, Y., Zhou, X.-D., Xu, H. H., Weir, M. D., Zhang, K.-K., et al. (2016). Effect of Anti-Biofilm Glass-Ionomer Cement on Streptococcus Mutans Biofilms. *Int. J. Oral Sci.* 8 (2), 76–83. doi:10.1038/ijos.2015.55

Wiegand, A., Buchalla, W., and Attin, T. (2007). Review on Fluoride-Releasing Restorative Materials-Fluoride Release and Uptake Characteristics, Antibacterial Activity and Influence on Caries Formation. *Dental Mater.* 23 (3), 343–362. doi:10.1016/j.dental.2006.01.022

Xu, H. H. K., Moreau, J. L., Sun, L., and Chow, L. C. (2010). Novel CaF(2) Nanocomposite with High Strength and Fluoride Ion Release. *J. Dent Res.* 89 (7), 739–745. doi:10.1177/0022034510364490

Yamakami, S. A., Ubaldini, A. L. M., Sato, F., Medina Neto, A., Pascotto, R. C., and Baesso, M. L. (2018). Study of the Chemical Interaction between a High-Viscosity Glass Ionomer Cement and Dentin. *J. Appl. Oral Sci.* 26, e20170384. doi:10.1590/1678-7757-2017-0384

Yesilyurt, C., Er, K., Tasdemir, T., Buruk, K., and Celik, D. (2009). Antibacterial Activity and Physical Properties of Glass-Ionomer Cements Containing Antibiotics. *Oper. Dent* 34 (1), 18–23. doi:10.2341/08-30

Yue, Y., Zeng, L., Wang, X., Su, L., Sun, M., Wu, B., et al. (2019). Loading of AgNPs onto the Surface of boron Nitride Nanosheets for Determination of Scopoletin in Atractylodes Macrocephala. *Sci. Rep.* 9 (1), 3864. doi:10.1038/s41598-019-40511-y

Zhang, K., Wang, S., Zhou, X., Xu, H. H. K., Weir, M. D., Ge, Y., et al. (2015). Effect of Antibacterial Dental Adhesive on Multispecies Biofilms Formation. *J. Dent Res.* 94 (4), 622–629. doi:10.1177/0022034515571416

Zhang, R., and Gao, L. (2001). Effect of Peptization on Phase Transformation of TiO2 Nanoparticles. *Mater. Res. Bull.* 36 (11), 1957–1965. doi:10.1016/S0025-5408(01)00674-2

Conflict of Interest: The authors declare that the research was conducted in the absence of any commercial or financial relationships that could be construed as a potential conflict of interest.

Publisher's Note: All claims expressed in this article are solely those of the authors and do not necessarily represent those of their affiliated organizations, or those of the publisher, the editors and the reviewers. Any product that may be evaluated in this article, or claim that may be made by its manufacturer, is not guaranteed or endorsed by the publisher.

Copyright © 2022 Ma, Guo, Liu, Wang, Yang, Kong, Jia, Li, Han, Zheng, Hu and Liu. This is an open-access article distributed under the terms of the Creative Commons Attribution License (CC BY). The use, distribution or reproduction in other forums is permitted, provided the original author(s) and the copyright owner(s) are credited and that the original publication in this journal is cited, in accordance with accepted academic practice. No use, distribution or reproduction is permitted which does not comply with these terms.